Noise-equivalent and signal-equivalent visual summation of quantal events in space and time

Hemilä, S.

Cambridge University Press
1998

Visual Neuroscience. 1998. 15: 731-742

http://hdl.handle.net/1975/949

Visual Neuroscience (1998), **15**, 731–742. Printed in the USA.

Noise-equivalent and signal-equivalent visual summation of quantal events in space and time

SIMO HEMILÄ,[1] TUOMO LERBER,[1] AND KRISTIAN DONNER[2]

[1]Laboratory of Physics, FIN-02015 Helsinki University of Technology, Espoo, Finland
[2]Department of Biosciences, FIN-00014 University of Helsinki, Helsinki, Finland

(RECEIVED July 16, 1997; ACCEPTED January 12, 1998)

Abstract

Noise recorded in visual neurons, or variability in psychophysical experiments, may be quantified in terms of quantal fluctuations from an "equivalent" steady illumination. The conversion requires assumptions concerning how photon signals are pooled in space and time, i.e. how to pass from light *fluxes* to *numbers* of photon events relevant to the Poisson statistics describing signal/noise. It is usual to approximate real weighting profiles for the integration of photon events in space and time (the sensitivity distribution of the receptive field [RF] and the waveform of the impulse response [IR]) by sharp-bordered apertures of "complete," equal-weight summation of events. Apertures based on *signal-equivalence* cannot provide *noise-equivalence*, however, because greater numbers of events summed with smaller weights (as in reality) have lower variances than smaller numbers summed with full weight. Thus sharp-bordered apertures are necessarily smaller if defined for noise- than for signal-equivalence. We here consider the difference for some commonly encountered RF and IR profiles. *Summation areas*, expressed as numbers of photoreceptors (cones or rods) contributing with equal weight, are denoted N_S for signal and N_N for noise; sharply delimited *summation times* are correspondingly denoted t_S and t_N. We show that the relation in space is $N_N = 0.5N_S$ for the Gaussian distribution (e.g. for the RF center mechanism of retinal ganglion cells). For a photoreceptor in an electrically coupled network the difference is even larger, e.g., for rods in the toad retina $N_N = 0.2N_S$ ($N_S = 13.7$ rods and $N_N = 2.8$ rods). In time, the relation is $t_N \approx 0.7t_S$ for realistic quantal response waveforms of photoreceptors. The surround input in a difference-of-Gaussians RF may either decrease or increase total noise, depending on the degree of correlation of center and surround noise. We introduce a third useful definition of sharp-bordered summation apertures: one that provides the same signal-to-noise ratio (SNR) for large-long stimuli as the real integration profiles. The *SNR-equivalent* summation area is $N^* = N_S^2/N_N$ and summation time $t^* = t_S^2/t_N$.

Keywords: Photoreceptor, Retina, Quantal fluctuation, Signal-to-noise ratio, Receptive field, Vision

Introduction

It is often useful to calibrate signal-to-noise ratios (SNRs) recorded in visual neurons or in psychophysical experiments against the "extrinsic" SNR of the light signal, the absolute physical limit, where the only source of variation is the statistical fluctuations in the photon flux (de Vries, 1943; Barlow, 1957). An obvious extension of this is to quantify extra, "biological" variability in terms of quantal fluctuations from a hypothetic "intrinsic" background light (Barlow, 1956, 1964, 1977). However, quantal fluctuations follow the Poisson statistics of *numbers*, while light usually arrives as a continuous *flux*, so the correspondence between photon fluctuations and biological variability will depend on how that flux is chopped into spatio-temporal packages. This is frequently done by defining sharply delimited summation areas and times, such that photons falling within these are assumed to be summed with equal weight, while photons falling outside do not contribute at all to a particular spatio-temporal "pixel." The realistic biological descriptors are the sensitivity profile of the receptive field (RF) in space and the waveform (persistence profile) of the quantal response (or impulse response, IR) in time. The sharp-bordered apertures are defined so that they contain the same integrated light sensitivity as the real profiles and, within the borders, have constant sensitivity equal to the peak sensitivity of the real profiles (see Fig. 1). The psychophysical precedents are Riccò's (1877) law of spatial summation, integrated into neurophysiology by Adrian and Matthews (1927) and Hartline (1940), and Bloch's (1885) law of temporal summation, related to photoreceptor responses by Baylor and Hodgkin (1973).

We here consider the errors that arise when such apertures defined for *signal-equivalence* are used for calculating *noise-equivalent* intrinsic lights from biological variability, or conversely, for calculating expected biological variability under the assumption that quantal fluctuation of the real light is the only

Address correspondence and reprint requests to: Kristian Donner, Department of Biosciences, P.O. Box 17 (Arkadiankatu 7), FIN-00014 University of Helsinki, Finland.

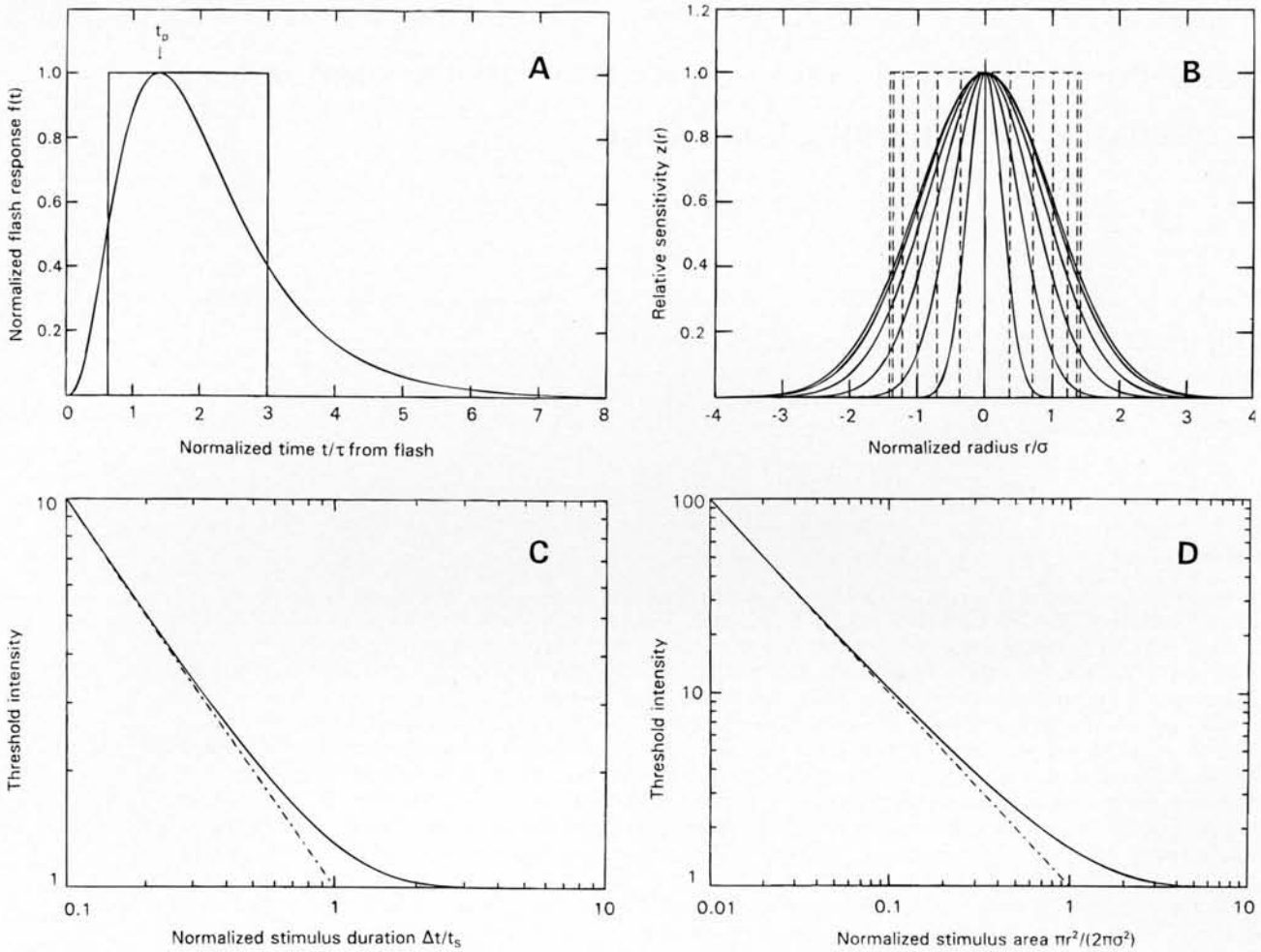

Fig. 1. Schematic presentation of the relation between realistic temporal and spatial weighting profiles and corresponding sharp-bordered summation apertures. A: Waveform of the response to a single photoisomerization according to the "independent activation model" (with $n = 4$), and the signal-equivalent rectangular response. The base of the rectangle is t_S (here = $1.71t_p$), and its area is equal to the area under the smooth waveform. B: Two-dimensional Gaussian spatial sensitivity distribution (standard deviation = σ) and the signal-equivalent cylindrical, "top-hat" sensitivity distribution (dashed lines). The radius of the latter is $r_S = \sigma\sqrt{2}$, and its volume is equal to that of the Gaussian. C: Duration-threshold function, i.e. log stimulus duration versus log threshold intensity for the quantal response in (A). The point of intersection of the 45 deg and horizontal asymptotes (straight lines of slopes −1 and 0) is the signal-equivalent summation time t_S (= 1 on the normalized abscissa). This is a usual method for determining the interval of "complete" temporal summation (Bloch's interval, also called the Bunsen-Roscoe range). Note that t_S can be obtained from only two threshold measurements: one for a very brief stimulus ($\ll t_S$) and one for a very long stimulus ($\gg t_S$), fixing the vertical positions of the two asymptotes. D: Area-threshold function, i.e. log stimulus area versus log threshold intensity for the Gaussian RF in (B). The point of intersection of the 45 deg and the horizontal asymptotes (straight lines of slopes −1 and 0) is the signal-equivalent summation area A_S (= 1 on the normalized abscissa). This is a usual method for determining the area of "complete" spatial summation (Riccò's area). Note that A_S can be obtained from only two threshold measurements, one for a very small stimulus area ($\ll A_S$) and one for a very large stimulus area ($\gg A_S$), fixing the vertical positions of the two asymptotes.

noise source. The point of departure is the fact that experimentally observed RFs or IRs never have sharp borders, but rise and fall more or less gradually. Replacing these by rectangular profiles means that the signal is construed as being built from a smaller number of quantal events summed with peak weight, compared with the real situation where a larger number of events contribute with individual, generally smaller weights. The same transformation cannot hold for noise, because the relative variation due to the larger number of smaller events is necessarily lower than that due to the smaller number of full-sized events. If recorded variability is expressed in terms of fluctuations of standard-sized quantal events, these will appear to be collected over smaller areas and shorter times than those that constitute the signal. Our purpose is to clarify how significant the difference is for some commonly encountered spatial and temporal integration profiles, particularly with a view to assessing potential errors in earlier "dark light" estimates.

The analysis is not restricted to the profiles taken as examples here, but could easily be extended to any spatial and temporal weighting profiles of linear detectors. Nor is it basically limited to Poisson variances connected with photon statistics, but shows quite generally how random neural fluctuations, as opposed to common-

mode signals, add in space and time. It further suggests a fast way of obtaining information on unknown weighting profiles by measuring summation apertures for externally added dynamic noise in its effect on detection thresholds (e.g. image noise in psychophysical detection tasks).

Theory and results

Signal-equivalent summation apertures

Temporal

A photoisomerization elicits a quantal response of standard waveform in a photoreceptor cell (e.g. Pugh & Lamb, 1990) (rod or cone; for brevity, we shall generally talk about "rods," although most of the considerations apply equally well to cones). This waveform may be viewed as a "persistence profile," describing the relative strength of the effect of an isomerization at each point in time after it has occurred. Our purpose is to replace that profile by a rectangular one, as if the effect persisted at a constant (maximal) level for such a time that the total (integrated) effect is the same as for the real profile. The general idea is illustrated in Fig. 1A for one particular persistence profile (see further below).

Let $f(t)$ be the relative amplitude of the quantal response as function of time after the isomerization, with $f(t) = 1$ at the peak of the response. The same integrated effect is provided by a rectangular pulse of amplitude = 1 and the duration t_S given by (Baylor & Hodgkin, 1973):

$$t_S = \int_0^\infty f(t)\,dt \tag{1}$$

This corresponds to the "interval of complete summation": the signal at any moment can be construed as the sum of equal contributions from all isomerisations that have occurred within the preceding time window t_S (Bloch, 1885; cf. Baumgardt, 1972). We term it the *signal-equivalent summation time*. It is identical to the "critical duration" of a stimulus pulse, determined as the point of intersection of two straight lines of slopes -1 and 0 fitted to log pulse duration–log threshold intensity data (Fig. 1C). This method for determining t_S, by recording threshold intensity as function of stimulus duration, has been widely used both in psychophysics and neurophysiology. Results of several psychophysical studies of this kind are summarized in Table 2 of Donner et al. (1995).

The waveform of the quantal response in many rods and cones is well described by the "independent activation" model of Baylor et al. (1974):

$$f(t) = S_I \exp(-t/\tau)\,[1 - \exp(-t/\tau)]^{n-1} \tag{2}$$

where n is the number of stages in the filter chain, τ is the largest of the time constants (the rate constants $1/\tau$ of the stages forming an arithmetic sequence), and S_I is a normalizing factor scaling the amplitude to unity at peak. Thus, $f(t_p) = 1$, where $t_p = \tau(\ln n)$ is the time to peak. The summation time corresponding to this waveform, obtained by substituting eqn. (2) into eqn. (1), is $t_S = \tau[n/(n-1)]^{n-1}$. For physiologically realistic values of n, this ranges from $t_S = 1.30t_p$ (for $n = 7$) to $t_S = 1.71t_p$ (for $n = 4$). In Fig. 1A, the relation between $f(t)$ and the signal-equivalent summation time is illustrated for "independent activation" kinetics with $n = 4$.

In some rods and cones, the quantal response is better described by the "Poisson" model of Baylor et al. (1974):

$$f(t) = S_P t^{n-1} \exp(-t/\tau) \tag{3}$$

where τ is the time constant (same for all stages in the filter chain) and S_P is again a normalizing factor scaling the amplitude of the response to unity at peak. Thus, $f(t_p) = 1$, where $t_p = (n-1)\tau$ is the time to peak. The summation time for Poisson kinetics, obtained by substituting eqn. (3) into eqn. (1), is $t_S = \tau[e/(n-1)]^{n-1}(n-1)!$. For physiologically realistic values of n, this ranges from $t_S = 1.04t_p$ (for $n = 7$) to $t_S = 1.49t_p$ (for $n = 4$).

Spatial

We assume for simplicity that the RF sensitivity distribution is circularly symmetric and that the quantal signals from rods add linearly. Sensitivity is maximal in the RF midpoint and decreases towards zero according to some continuous function of distance from there. The relative sensitivity at the distance r is denoted $z(r)$, with $z(0) = 1$ and $z(\infty) = 0$. We consider responses to full-field stimuli. If U_0 is the amplitude of a signal elicited by one photoisomerization in a rod at the RF midpoint, a photoisomerization in rod n at the distance r_n elicits a signal $U_0 z(r_n)$ and [writing $z(r_n)$ as z_n] the total signal is $U_0 \Sigma z_n$. Obviously, the same *response* would be elicited by Σz_n rods if all of them contributed a maximum-sized response (if all had $z = 1$). Thus, $N_S = \Sigma z_n$ is the number of rods contributing with equal (full) weight that together would give the same response to full-field illumination as does the real RF. If the retinal rod density is ρ, the effective area occupied by these is $A_S = N_S/\rho$ or

$$A_S = \int_0^\infty z(r) 2\pi r\,dr \tag{4}$$

This is the "area of complete summation" or the *signal-equivalent summation area* (Riccò's area). Cylindrical ("rectangular") weighting profiles are commonly referred to as "top-hats," and the one with base area A_S may be termed the *signal-equivalent top-hat receptive field* (STRF). The relation between the real weighting profile and the STRF is illustrated in Fig. 1B for one particular case (the Gaussian).

One commonly used method for measuring spatial summation characteristics is by recording the "area-threshold function," i.e. threshold intensity as function of the area of a circular incremental stimulus. A_S is obtained as the point of intersection of two straight lines of slopes -1 and 0 fitted to the log–log data (Cleland & Enroth-Cugell, 1968; Donner & Grönholm, 1984). This is exemplified in Fig. 1D for the Gaussian case.

Example 1: Gaussian receptive fields. The two-dimensional Gaussian distribution provides a good description of the RF sensitivity profile of many types of visual neurons, e.g. horizontal cells and both the center and the surround mechanisms of ganglion cells in the retina, but also appears as a weighting function, e.g. in Gabor-type RFs commonly assumed in psychophysics. For a two-dimensional Gaussian distribution with standard deviation σ

$$A_S = \pi r_S^2 = \int_0^\infty \exp(-r^2/2\sigma^2) 2\pi r\,dr = 2\pi\sigma^2 \tag{5}$$

Thus, the radius of the STRF approximation of a Gaussian is $r_S = \sigma\sqrt{2}$ (Fig. 1B).

Example 2: Receptive fields with Bessel flanks. Rods of at least lower vertebrates are electrically coupled, so the response in each rod contains contributions from many neighbors (Schwartz, 1975; Fain, 1975; Fain et al., 1976). The sensitivity profile has a sharp apex in the central rod but a wide spread, deviating much more strongly from a top-hat than does the Gaussian. The rod mosaic can be modelled as a homogeneous syncytium (Lamb & Simon, 1976; Schwartz, 1976; Fain et al., 1976; Attwell & Wilson, 1980; Tessier-Lavigne & Attwell, 1988) with two essential parameters: the leakage conductance from the syncytium interior to exterior per unit area, denoted G_s (S/m^2), and the longitudinal resistance of the unit area, denoted R_s. The sensitivity profile of the flanks can then be described by a modified Bessel function of the second kind, K_0 (Minor & Maksimov, 1969; Lamb & Simon, 1976):

$$z(r) = K_0(r/\lambda) \tag{6}$$

where $\lambda = 1/\sqrt{R_s G_s}$ is the space constant of the syncytium. The response of a rod to one photoisomerization occurring in another rod at the distance r is then

$$U = U_B K_0(r/\lambda) \tag{7}$$

where U_B is a constant. This *continuous* model based on a homogeneous syncytium breaks down when r approaches zero, as is intuitively obvious from the fact that very small radii will be wholly contained within one single rod (the central rod), and as is mathematically evident from the fact that $K_0(0)$ is infinite. For small values of r, it is necessary to take into account the *discrete* nature of the rod network. This entails, e.g. assigning a finite value to $z(0)$.

The STRF approximation depends on λ and $z(0)$. We defer calculation of the summation area to the simulations in the last section of the Results and the Appendix, with parameters representative of the rod network of the toad retina.

Noise-equivalent summation apertures

Temporal

Assume that there is a steady illumination and/or an intrinsic background "light," producing I_0 isomerizations per rod per second (Rh^*s^{-1}) on average. The response to isomerizations (j) occurring at times t_j in one rod (n) at the distance r_n from the RF midpoint is

$$U_n(t) = z(r_n) U_0 \sum_j f(t - t_j) \tag{8}$$

where U_0 is the response amplitude to an isomerization in the middle of the RF [$z(0) = 1$]. According to Campbell's theorem (see e.g. Van der Ziel, 1970), the variance of $U_n(t)$ is

$$\sigma_n^2 = I_0 z_n^2 U_0^2 \int_0^\infty f(t)^2 \, dt \tag{9}$$

The integral in eqn. (9) captures the temporal persistence of the *noise* effects of the isomerizations. By analogy with the definition of a "signal-equivalent summation time" t_S [eqn. (1)], we thus define a *noise-equivalent summation time* t_N:

$$t_N = \int_0^\infty f(t)^2 \, dt \tag{10}$$

The Poisson variance of the number of events falling in this time window, when multiplied by $I_0 z_n^2 U_0^2$, is equal to the recorded neural variance. It is informative to express t_N as a fraction κ of the signal-equivalent summation time t_S [cf. eqn. (1)]:

$$t_N = \int_0^\infty f(t)^2 \, dt = \kappa \int_0^\infty f(t) \, dt = \kappa t_S \tag{11}$$

If the actual waveform $f(t)$ were rectangular, κ would of course be = 1. If $f(t)$ follows "independent activation" kinetics [eqn. (2)], $\kappa \approx 0.68$; in this case varying the parameter n (the number of stages in the filter chain) in a realistic range ($n = 4$–7) has only minor effects on κ. If $f(t)$ follows "Poisson" kinetics [eqn. (3)], κ depends somewhat more strongly on n, growing monotonically from *ca.* 0.71 at $n = 4$ to *ca.* 0.80 at $n = 7$.

Spatial

The random voltages from different rods are uncorrelated. Thus, the total variance caused by the steady "background" illumination (denoted σ_B^2) is the sum of the variances σ_n^2 from all contributing rods,

$$\sigma_B^2 = \Sigma\sigma_n^2 = I_0 U_0^2 \kappa t_S \Sigma z_n^2 \tag{12}$$

Our purpose, to produce the same total variance by means of N_N rods that all contribute with equal weight, is achieved if

$$N_N = \Sigma z_n^2 \tag{13}$$

The area encompassing this number of rods is $A_N = N_N/\rho$ or, assuming that it is circular:

$$A_N = \int_0^\infty z^2(r) 2\pi r \, dr \tag{14}$$

This is the general expression for the base area of what we term the *noise-equivalent top-hat RF* (NTRF). For the Gaussian profile this gives

$$A_N = \int_0^\infty \exp(-r^2/\sigma^2) 2\pi r \, dr = \pi\sigma^2 \tag{15}$$

and comparison with eqn. (5) shows that $N_N = 0.5 N_S$. Thus, if the real RF profile is Gaussian, the noise power would be accounted for by Poisson fluctuations in half the number of equal-weight rods that have to be invoked to build up the signal. If noise were summed from the signal-equivalent number of rods (the STRF), it would be much more powerful than in reality (Fig. 2). This reflects the advantage of "smooth" weighting profiles for viewing natural scenes (see Discussion). To decrease noise in a top-hat RF to the same level as in the Gaussian RF, the former would have to be

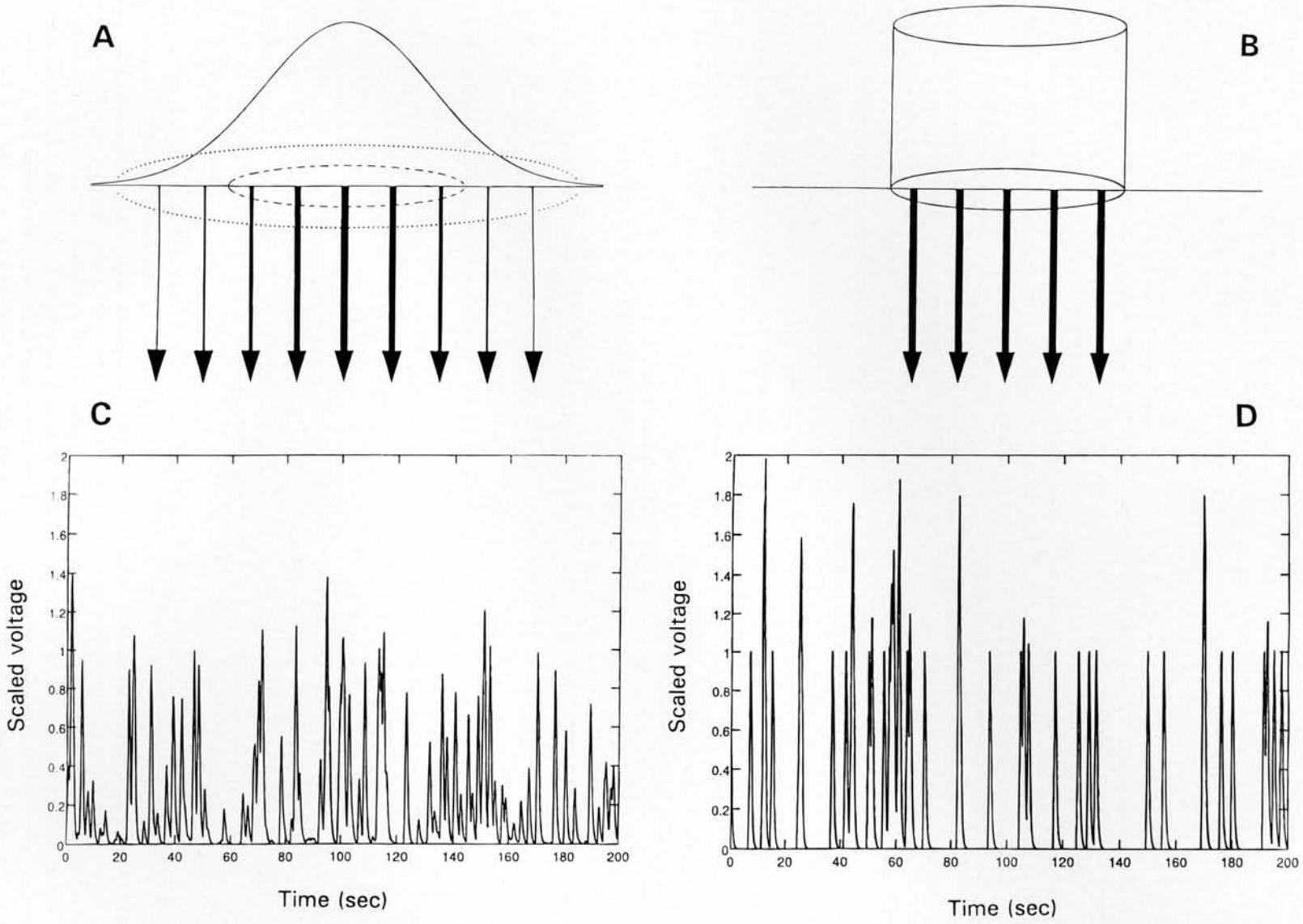

Fig. 2. Simulation of the noise elicited by a steady full-field background light in a Gaussian RF and a top-hat RF that would give identical mean responses to full-field (diffuse) light stimuli (e.g. light pulses or sinusoidal flicker). A,B: Schematic illustration of the two weighting distributions considered (A) Gaussian, and (B) the signal-equivalent top-hat. The base of the latter is a circle whose area is A_S (the summation area), reproduced as a dashed contour in (A). The dotted contour in (A) marks a circle with twice larger radius. The arrowheads stand for photoreceptors, and the thickness of the vertical lines symbolizes the strength of synaptic connection between a particular photoreceptor and the ganglion cell. C,D: Simulated noise over 200 s when the two types of RF are exposed to a steady full-field background light assumed to produce 0.21 photoisomerizations per A_S per second.

expanded by twofold (r would have to be increased by the factor $\sqrt{2}$ or *ca.* 40%), compromising spatial resolution.

The RF with Bessel flanks [eqn. (6)] differs much more from a top-hat than does the Gaussian, so the ratio N_N/N_S will be even smaller. In the last section of the Results, we will consider simulations showing that $N_N \approx 0.2N_S$ when calculated with parameters derived from the rod network of the toad retina.

Signal/noise-equivalent summation apertures

The use of sharp-bordered summation apertures is particularly convenient in calculations of SNRs limited by quantal noise. Assume that full-field "step" stimuli of intensity I_S (Rh^*s^{-1}) are given to an RF comprising N photoreceptors from which photon events are summed with equal weight over a time window T. (By a "step" stimulus we mean a rectangular pulse of any duration $\Delta t > T$.) The signal is then $U_0 I_S NT$. In the presence of a background event rate I_0 (which in general will be the sum of both an intrinsic "dark light" I_D and a real background light I_B), the average number of photon events in the receptive field within one summation time after stimulus onset is $NT(I_S + I_0)$. It has been customary to take the square root of this number, $\sqrt{NT(I_S + I_0)}$, as a measure of the Poisson quantal noise, which gives the SNR (Barlow, 1957, 1958, 1964; Copenhagen et al., 1987).

$$\mathrm{SNR} = \frac{NTI_S}{\sqrt{NT(I_S + I_0)}} = \sqrt{NT}\,\frac{I_S}{\sqrt{I_S + I_0}} \tag{16}$$

Although this equation is useful in showing that the SNR will be affected by changes in spatio-temporal summation, the above analysis demonstrates that it does not in general describe the SNR of an arbitrary linear filter in which $z(r)$ and $f(t)$ deviate from rectangular profiles. To achieve this, we rewrite the equation with N_S and t_S in the numerator and N_N and t_N in the denominator:

$$\mathrm{SNR} = \frac{N_S t_S I_S}{\sqrt{N_N t_N (I_F + I_0)}} = \sqrt{\frac{N_S^2 t_S^2}{N_N t_N}}\,\frac{I_S}{\sqrt{I_S + I_0}} \tag{17}$$

This, however, can be made formally identical to eqn. (16) by the introduction of new spatial and temporal summation apertures: $N^* = N_S^2/N_N$ and $t^* = t_S^2/t_N$, which we term *SNR-equivalent*. For a Gaussian sensitivity distribution, $N^* = 2N_S$. For the usual multistage filter waveforms of quantal responses (see above), $t^* \approx 1.4t_S$. With these SNR-equivalent parameters, the dependence of signal/noise on spatio-temporal summation can be written in a simple and accurate manner:

$$\mathrm{SNR} = \sqrt{N^* t^*} \cdot I_S / \sqrt{(I_S + I_0)} \tag{18}$$

Summation of noise in difference-of-Gaussian receptive fields

Retinal ganglion cells and many other higher order neurons (even cone photoreceptors in some species) receive antagonistic input from "surround" mechanisms with their own spatial profiles weighting the primary photoreceptor signals. Generally, RF profiles of surround mechanisms are wider and have lower peak sensitivity than "center" profiles. Of particular interest is the *difference-of-Gaussians* (DOG) RF, which successfully accounts for many properties of linear retinal ganglion cells (see e.g. Troy, 1993). For modelling purposes, it is reasonable to assume that both center and surround are circularly symmetric and concentric Gaussians, and that the output at each moment is the center signal minus the surround signal relatively lagged by a fixed delay. This model has been shown to work well for *photoresponses* to e.g. sinusoidal contrast modulation (Enroth-Cugell et al., 1983; Donner & Hemilä, 1996). Our present concern is how the *noise* transmitted from photoreceptors over the "additional" surround pathway will affect total noise in the ganglion cell.

In general, noise arriving over the center and surround pathways will show some degree of correlation, as both mechanisms take their primary input at least partly from the same set of photoreceptors (in the middle part of the RF). Despite this, it is instructive to consider first the (admittedly restrictive) assumption that the two noise components are uncorrelated. This situation would be approximated, e.g. (1) if there is strong variability in the transmission times from photoreceptors to the ganglion cell over one or both of the pathways, (2) if the relative surround delay is large compared with the summation time of the photoreceptors (see below), or (3) if the proportion of common photoreceptor input is small, either because the surround is much wider than the center, or because the two mechanisms selectively contact different subsets of photoreceptors (as e.g. in color-opponent cells).

Uncorrelated noise

Let the subscript c refer to the center and the subscript a to the antagonistic surround. The total noise standard deviation will be $\sigma_{DOG} = \sqrt{\sigma_c^2 + \sigma_a^2}$. According to eqns. (12) and (13), variance σ^2 is proportional to $N_N U_0^2$. In a *balanced* DOG RF, where the integrated weighting functions of the center and the surround are equal, the voltages $I_0 t_S N_S U_0$ of the two mechanisms are equal (see Donner & Hemilä, 1996), implying that $U_{0a}/U_{0c} = N_{Sc}/N_{Sa}$. The ratio of variances in a balanced DOG RF is therefore

$$\begin{aligned}\sigma_a^2/\sigma_c^2 &= N_{Na} U_{0a}^2 / N_{Nc} U_{0c}^2 \\ &= (N_{Na}/N_{Nc})(N_{Sc}/N_{Sa})^2 = N_{Sc}/N_{Sa}\end{aligned} \tag{19}$$

and the surround input increases the total standard deviation by the factor

$$\sigma_{DOG}/\sigma_c = \sqrt{(1 + N_{Sc}/N_{Sa})} = \sqrt{(1 + r_{Sc}^2/r_{Sa}^2)} \tag{20}$$

When $r_{Sc} = r_{Sa}$ (center and surround coextensive), this factor is $\sqrt{2}$, i.e. the surround increases noise by *ca.* 40%. However, when $r_{Sa} = 1.5r_{Sc}$ the increase due to the surround is only 20% and if $r_{Sa} = 3r_{Sc}$ no more than *ca.* 5%. The "cost" of center-surround organization in terms of extra noise quickly becomes negligible as the surround grows larger.

Correlated noise

Given the relative insignificance of surround noise for large r_{Sa} even if noise in the two pathways is completely uncorrelated, we focus the analysis of correlated noise on the situation $r_{Sc} = r_{Sa}$. We further assume maximal correlation, i.e. that center and surround sample exactly the same set of photoreceptors and that the center-surround transmission delay d has a fixed value, with no variation. As before, the RF is a balanced DOG. An analytical solution is readily available for a "difference of top-hats" (see Van der Ziel, 1970), but for the DOG RF, we here prefer to do simulations rather than develop extensive mathematical formalism. In the simulations

we assumed spatio-temporally random arrival of photons, each producing a response with four-stage "independent activation" kinetics in rods. We determined by what factor (σ_{DOG}/σ_c) the surround input multiplies total noise. The result is critically dependent on the value of d *relative* to the time scale of the photoreceptor response, which can be captured in the summation time t_S. Therefore, Table 1 tabulates results for different values of center-surround delays *scaled* by t_S.

When the center-surround delay is large ($d/t_S > 1$), noise from the two mechanisms becomes practically uncorrelated, and σ_{DOG}/σ_c converges towards eqn. (20). In a midrange of d/t_S (around 0.5), the total noise power is not much different from that of a single Gaussian ($\sigma_{DOG}/\sigma_c \approx 1$). For smaller delays, however, the surround input significantly *decreases* total noise. This is because the delayed but strictly correlated antagonistic input curtails the single events. In effect, the surround then serves as a high-pass filter, decreasing the gain of the system at low to medium temporal frequencies (see Fig. 3 in Donner & Hemilä, 1996). Which of the d/t_S values in Table 1 would be physiologically realistic? Our best guesses range from about 0.5 for light-adapted cones to 0.1 or even lower for dark-adapted rods (Donner & Hemilä, 1996). Over this whole range, the RF surround will decrease the total power of photoreceptor-originated noise in the ganglion cell. Implications for SNRs will depend on the type of stimulus to be detected and the nature of the detection process (see Discussion).

We have also performed simulations where the center-surround delay d was allowed to vary. For large standard deviations ($>t_S$) of d, center and surround noise become increasingly uncorrelated, and σ_{DOG}/σ_c converges towards eqn. (20). Smaller variability in a physiologically realistic range (see Baylor & Fettiplace, 1977) has little effect, however.

Table 1. *Simulated noise in a balanced DOG RF, assuming that center and surround receive their input from the same set of photoreceptors, for different values of the (normalized) center-surround delay* (d/t_S)[a]

d/t_S	σ_{DOG}/σ_c	U_{DOG}/U_0	SNR_{rel}
0.05	0.11	0.15	1.41
0.1	0.21	0.30	1.40
0.2	0.41	0.56	1.37
0.3	0.58	0.77	1.32
0.4	0.74	0.91	1.22
0.5	0.88	0.98	1.11
0.6	0.99	1.00	1.01
1.0	1.35	1.00	0.74
3.5	1.42	1.00	0.70

[a]Total noise standard deviation in a DOG RF is given as fraction of the noise standard deviation in a single-Gaussian RF (corresponding to the center mechanism alone) under the same conditions (σ_{DOG}/σ_c). The third column gives the amplitude of the quantal response in the DOG RF as a fraction of the amplitude of the quantal response without antagonistic surround. The fourth column gives the SNR for response-amplitude-based detection of a brief dim flash of light in the DOG RF relative to that in the single Gaussian. The noise values are means of results from 100 simulated noise periods, each of which represented a 200-s exposure to a steady (Poisson-distributed) photon flux producing on average 0.21 isomerizations in the RF per second. The quantal response was assumed to have independent activation kinetics with $n = 4$. See text for further details.

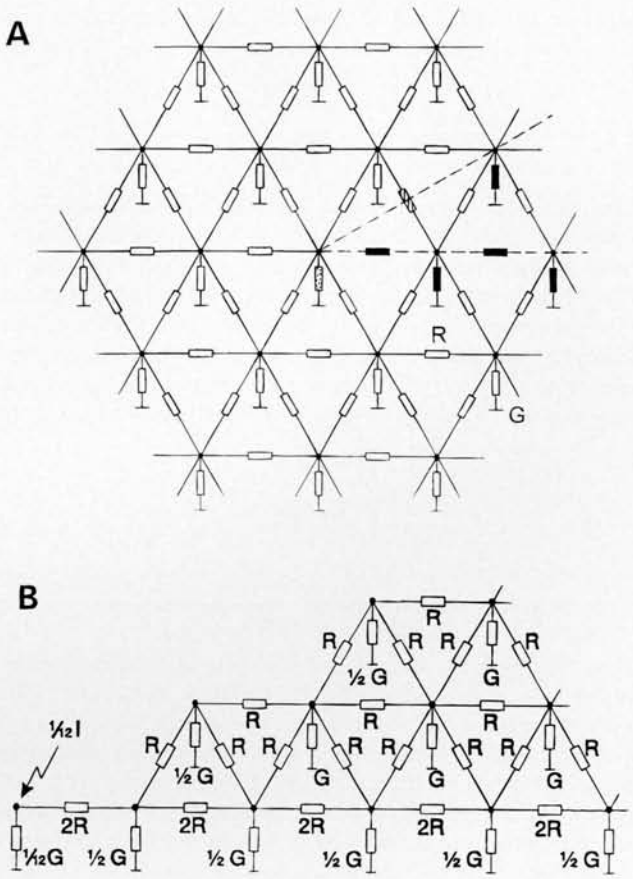

Fig. 3. A: A piece of hexagonal rod lattice. R is the resistance between nearest neighbors and G is the leakage conductance from each rod interior to exterior. The photocurrent is injected into the central rod (where the leakage conductance is shown as stipled). The lattice may be divided into 12 identical sectors, as illustrated by the dashed lines delimiting one such sector. The resistances and conductances on the border of that sector, shown in black, belong to two sectors, while the central conductance belongs to all 12 sectors. Resistances orthogonal to sector borders (one of which is shown as striped) may be omitted, because no current flows across the border. B: The central part of the equivalent circuit of one sector of the hexagonal lattice used in the calculations.

Determining RF size by recording the mean and variance of responses

Theory

Sensitivity and variance information may, conversely, be used for *determining* the effective size of summation apertures. For example, Copenhagen et al. (1990) measured the mean amplitude and variance of responses to brief, full-field flashes in toad rods and horizontal cells, assuming that intrinsic noise could be neglected. If the flash produces I_F photoisomerizations per rod (Rh^*) and signals are summed from N rods, the mean response is $U = U_0 I_F N$. Copenhagen et al. took $\sigma^2 = U_0^2 I_F N$ as the "expected" variance, and by eliminating U_0 obtained an expression for the number of rods contributing with equal weight:

$$N = U^2/(\sigma^2 I_F) \qquad (21)$$

However, this expression is ambiguous in the same way as eqn. (16) for the SNR. In fact, the response is $U = U_0 I_F N_S$ but the variance is $\sigma^2 = U_0^2 I_F N_N$. Elimination of U_0 then gives

$$U^2/(\sigma^2 I_F) = N_S^2/N_N = N^* \tag{22}$$

Thus, when this method is used, the value obtained is the *SNR-equivalent* number of rods. The same is true of another variance-based method, using responses to dim, full-field flashes ($U = U_0 I_F N_S$) and the voltage variance σ_B^2 recorded without flashes but in the presence of a dim background light I_B that constitutes the dominant noise source. According to eqns. (12) and (13) the variance is $\sigma_B^2 = I_B U_0^2 \kappa t_S N_N$. Denoting the sensitivity (the gain of the response) to full-field flashes $S_{FF} = U/I_F$ and eliminating U_0, we get

$$N^* = \frac{S_{FF}^2 I_B \kappa t_S}{\sigma_B^2} \tag{23}$$

Simulation of signal-equivalent, noise-equivalent and SNR-equivalent summation areas of toad rods

In the Appendix, we demonstrate the use of these methods by simulations on the rod network in the retina of the toad, *Bufo marinus*, to determine the three types of summation areas of a rod *in situ*. The rod RF is interesting for this purpose, as it differs very strongly from the top-hat profile, and in *Bufo marinus* the crucial parameters are known with reasonable accuracy. The simulations apply a special case of the discrete-component models developed by Lamb and Simon (1976) and Tessier-Lavigne and Attwell (1988) for calculating responses, noises, and input resistances of photoreceptors in coupled networks. The resulting weighting profile is a Bessel function except for a sharp peak of high but finite sensitivity in the central rod. The details are described in the Appendix.

First, we simulated the mean response of each rod to an isomerization in the central rod. From this simulation, we obtained the following values: $N_S = \Sigma z_n = 13.7$ rods, $A_S = N_S/\rho = 910\ \mu m^2$, $N_N = \Sigma z_n^2 = 2.8$ rods, and $N^* = N_S^2/N_N = 67$ rods. We then determined N^* by the alternative method of simulating the variance of responses to dim flashes [eqn. (22)]. Two simulations of this type yielded the values $N^* = 67.8$ and 66.9 rods. Finally, we determined N_N by simulating the noise from a weak, steady background illumination [eqn. (23)], obtaining $N_N = 2.73$ rods, in good agreement with the above value of 2.8 rods.

Discussion

Three kinds of spatial and temporal summation apertures

The signal in a linear neuron under full-field stimulation can always be translated into a sum of equal-weight signals from a certain number of rods, the *signal-equivalent* number N_S (thus $U_{tot} = N_S U_0$). In analogous manner, the noise can be construed as a sum of equal-weight contributions from a *noise-equivalent* number of rods, N_N. For any spatial weighting function with smooth flanks, $N_N < N_S$, as is qualitatively obvious from the following argument. The noise statistic that allows straightforward addition is *variance* (thus $\sigma_{tot}^2 = N_N \sigma_0^2$). Since variance is proportional to the *square* of amplitudes, and hence to the square of weighting factors z_n (≤ 1), the relative contributions of peripheral rods to variance will decrease faster than their contributions to the signal with increasing distance from the RF midpoint. Note further that N_N is *directly* proportional to variance, so somewhat counterintuitively and opposite to the case for N_S and N^*, increasing N_N implies decreasing SNR.

When the convenient and customary form of eqn. (16) is used for calculating SNRs, spatial summation must be described by the *SNR-equivalent* rod number $N^* = N_S^2/N_N$ [as in eqn. (18)]. The fact that $N_N < N_S$ and thus $N^* > N_S$ tells about the signal/noise advantage generally conferred by "smooth" RF profiles compared with the "top-hat" profile when the target to be detected is *not* a sharp-bordered circular spot matching the (top-hat) RF. This advantage is illustrated for diffuse illumination in Fig. 2, and it is almost universally present to some degree in natural vision because of the autocorrelation of brightness values in natural scenes and in the retinal image (cf. Srinivasan et al., 1982; Tsukamoto et al., 1990). For the top-hat RF to achieve the same SNR as the Gaussian RF in Fig. 2, it would have to be expanded by twofold (to cover N^* rods), which would instead degrade its capacity to resolve spatial detail.

We have explicitly dealt only with circularly symmetric RFs of retinal neurons, and not with, e.g. linear cortical receptive fields or other sensitivity profiles, as may be assumed in psychophysics. It should be observed, however, that similar considerations apply whenever signal and noise are calculated on the basis of photon statistics in equal-weight spatial elements, while the real weighting distribution has smoothly falling skirts. The analysis could be extended to any spatial weighting profile of linear detectors. Moreover, completely analogous arguments hold in the temporal domain for the three different summation times: t_S, t_N, and t^*.

Estimates of dark light per photoreceptor

When the number of isomerizations (photon or thermal) that would explain variability in a stage that sums from many rods (electrical noise in a visual neuron, or the variability of psychophysical detection) is referred back to single rods assumed to contribute with equal weight, it is essential that it be distributed on the noise-equivalent number N_N. If divided instead by the larger signal-equivalent number N_S, as has been usual, this will obviously give a misleadingly low value for the dark light in one rod cell. If the actual spatial weighting profile is Gaussian, the error is by a factor of 2. In analogous manner, the rate of dark events is underestimated by a factor of 1.4–1.5 if signal-equivalent rather than noise-equivalent summation times are used. If both these errors occurred together, the rate of dark photon-like events per photoreceptor per second would be underestimated by a factor of about 3.

Copenhagen et al. (1987), Aho et al. (1987), and Donner (1989) present distributions of noise-equivalent dark rates of photon-like events per rod in toad and frog, obtained from the response statistics and maintained discharge of retinal ganglion cells. Signal-equivalent summation apertures were used throughout, so the calculated event rates per rod are likely to be underestimates. The proportion of (studied) ganglion cells where the variability in light detection can be explained mainly by the statistics of photoisomerizations plus discrete "dark" isomerization-like events of the type first recorded in toad rods by Baylor et al., (1980) may thus be lower than the *ca.* 20% suggested in these studies.

Donner (1989) used the absolute sensitivities of 105 dark-adapted frog ganglion cells to calculate *expected* SNRs for threshold responses on the assumption that these are affected only by statistical variation in the number of flash-induced photoisomerizations plus the Baylor et al. (1980) type of dark events. In this inverse calculation, introduction of the appropriate, i.e. noise-

equivalent, apertures would *increase* expected SNRs. The correction would be important particularly in relation to the most sensitive 10% of the cells, which had "expected" threshold SNRs between 1 and 2 when calculated on the basis of signal-equivalent summation apertures (Donner, 1989). This appeared hard to reconcile with the experimenter's impression that thresholds were in reality "crisper" than would be suggested by such low SNR (low response reliability). Unfortunately, the number of trials in the majority of these threshold determinations had been too small to allow strictly quantitative estimates of variability.

RF size and the origin of noise in amphibian rods

The rod RF was analyzed in particular detail, as it deviates very strongly from the top-hat profile. Most of the $z(r)$ values obtained in the simulation agree with the function 0.3744 K_0 to within an accuracy of about 2% (Fig. 4). Excluding the midpoint, the largest deviation was 3.5% (second nearest neighbors, K_0 too large). The relative sensitivity curve $z(r)$ has a sharp apex in the midpoint. When $z(0)$ is set = 1, the six nearest neighbors have $z = 0.377$ and the second nearest neighbors $z = 0.217$. Even then, a quantal hyperpolarization in the central rod spreads so effectively that only about 7% of the total signal is sent directly to the second-order neuron, the rest being routed *via* other rods. This is functionally important, because the gain of transmission from rods to second-order cells is so high that without rod coupling the synapse would easily saturate (Attwell et al., 1987; Belgum & Copenhagen, 1988). For other functional aspects of the coupled photoreceptor network, see Lamb and Simon (1976) and Tessier-Lavigne and Attwell (1988).

The measurements of rod summation areas in *Bufo marinus* by Copenhagen et al. (1990) based on the mean-to-variance method yielded values ranging from 28 to 63 rods in seven cells, with a mean of 38 rods. As we have shown, what is obtained by this method is N^*, the SNR-equivalent number of rods. In their calculation, Copenhagen et al. assumed that intrinsic noise was negligible, just as we did in our present simulation. The fact that their experimental mean $N^* = 38$ rods is significantly lower than our simulated value, $N^* = 67$ rods, suggests the presence of nonnegligible intrinsic noise in the real rods. Still, it appears as more remarkable that clearly more than half of the recorded variation is accounted for by Poisson variation of the numbers of photoisomerizations in the rod RF.

Djupsund and Hariyama (1995) recorded rod voltage in the marsh frog *Rana ridibunda* in the presence of a known background light and determined the power spectrum integral, which is equal to σ_B^2 (Van der Ziel, 1970). Using eqn. (23), they obtained $N^* \approx 42$ (Djupsund, 1995), close to the value recorded in *Bufo marinus*.

The very small noise-equivalent summation area ($N_N = 2.8$ rods) found here for a *Bufo marinus* rod might at first sight seem to conflict with the conclusion of Lamb and Simon (1976) that "as far as the noise property is concerned, the responses of fifty cells are being averaged (when $a/\lambda = 0.54$)." In fact, there is no discrepancy, because Lamb and Simon compared the noise of a rod in the network and a rod in isolation. According to the top-hat model, the noise comes from N_N rods in the network, but in the network the input impedances and the voltages are reduced to a fraction $1/N_S$. Thus the voltage variance in the network is reduced by the factor N_N/N_S^2. This is the inverse of N^*, which is about 50 when $a/\lambda = 0.54$.

The effect of the surround in difference-of-Gaussians receptive fields

For *uncorrelated* center and surround noise, a unit with a DOG RF will always be noisier than one with an equal-sized simple Gaussian. In most cases, however, the noises arriving over the two path-

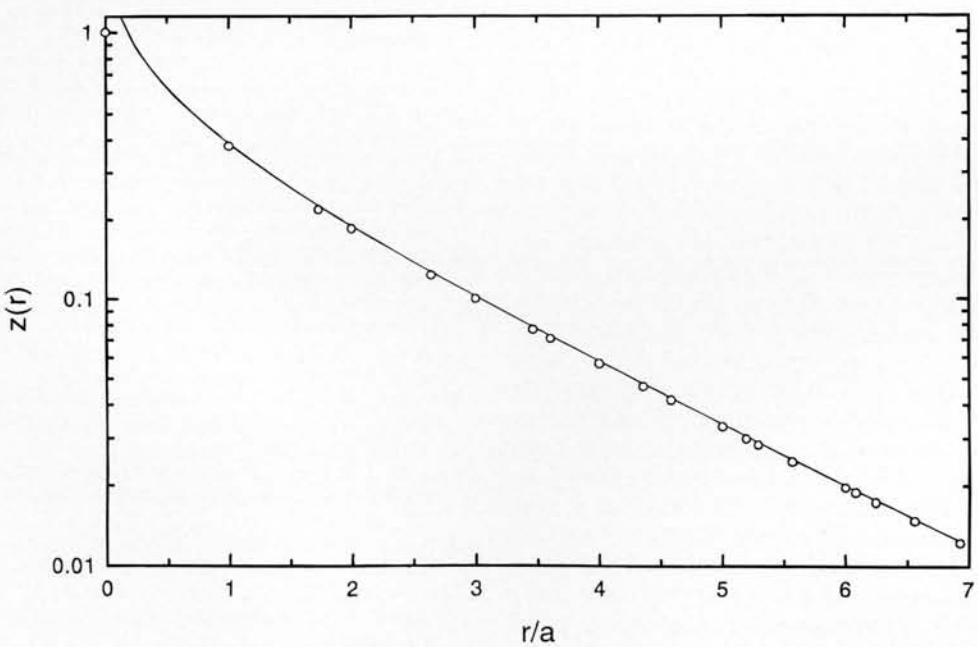

Fig. 4. The circles show the normalized responses of rods at different distances from the central rod in the hexagonal network. The line, representing the function 0.3744 $K_0(0.439r/a)$, has been fitted to the whole range $r/a = 0$–26 included in the simulations, but only the range $r/a = 0$–7 is shown.

ways will be at least partly correlated. Here we consider the consequences for the SNR under the assumption that surround noise exactly replicates center noise, only it is lagged by a constant delay.

If the system operates in a quantum-counting mode, as might be true close to the dark-adapted scotopic threshold, light detection is independent of the form of the quantal response. Thus, even allowing that surround mechanisms may be active down to very low illumination levels (cf. Enroth-Cugell & Lennie, 1975; Rovamo et al., 1998), the resulting modification of the quantal response waveform would in this case have no consequences—detection would still be limited by quantum statistics alone.

With more light, the surround effect might improve the detectability of some signals if detection is based on *signal amplitude*. For example, SNRs for the responses of DOG RFs to brief light flashes, relative to SNRs for responses of equal-sized simple Gaussian RFs, have been calculated in Table 1 as $(U_{DOG}/U_0)/(\sigma_{DOG}/\sigma_c)$, denoted SNR_{rel}. For $d/t_S = 0.1$, SNR_{rel} is 1.4, and for $d/t_S = 0.5$, $\mathrm{SNR}_{rel} = 1.11$. Thus the detectability of brief flashes would improve thanks to the surround (because it mainly attenuates lower temporal frequencies, whereas the amplitude of the flash response depends more on higher temporal frequencies). However, if detection is mediated by a temporal *matched filter*, the surround input has no direct effect on SNR: detection of a signal with a certain temporal-frequency composition is then limited only by noise of the same temporal-frequency composition, and the surround will (high-pass) filter the signal and the noise in exactly the same way at all temporal frequencies (Rovamo et al., 1996, 1998). This filtering is exemplified for two values of d/t_S (≈ 0.1 and ≈ 0.3) in Fig. 3 of Donner and Hemilä (1996). With respect to noise, the functional consequence of the surround mechanism would then simply be a general attenuation of low- and medium-frequency noise components of photoreceptor origin. This might contribute to the somewhat surprising unimportance of photon noise (i.e. dominance of neural noise originating more proximally in the system) in psychophysical detection tasks even at quite low illumination levels (Rovamo et al., 1998).

What the effect of externally added dynamic noise can tell about summation profiles

The analysis suggests a new type of experiment to characterize the spatial and temporal integration profiles of a noise-limited detector, analogous to the classical threshold *versus* stimulus area and threshold *versus* stimulus duration experiments (Figs. 1C and 1D). It is possible to add carefully calibrated amounts of dynamic spatial and/or temporal white noise over specified spatio-temporal windows in computer-generated stimulus images. The detection threshold for a small, briefly presented stimulus can thus be measured as a function of the spatial extent or temporal duration of the added noise (the stimulus always has to be fully contained within the noise window both in space and time). Under certain symmetry constraints, only two thresholds need to be measured: one for noise added exactly to the stimulus area (or presented for exactly the duration of the stimulus) and one for noise added over a "very large" area, much larger than A_N (or a "very long" noise duration, much longer than t_N). A_N and t_N are then obtained simply as points of intersection of two straight lines of slopes -0.5 and 0 drawn through the data points on log–log scales. For a given type of RF symmetry, e.g. circular, the spatial summation profile will largely be characterized by the ratio A_N/A_S. Correspondingly, t_N/t_S will tell much about the temporal summation profile.

Conclusions

Sharp-bordered apertures of "complete summation" remain useful models for how a visual neuron pools photons in space and time. They capture the extent of spatial or temporal summation in a single number, which can in principle be obtained from just two threshold determinations. The use of such summation areas and times for *signals* has a long tradition (Riccò, 1877; Bloch 1885), and Barlow (1957, 1958, 1964) expanded the concept to deal with the summation of (photon) *noise* liable to be confused with the signal. We have shown that for realistic weighting profiles with smoothly falling flanks, noise behaves as if summed over smaller areas and times than signals ($N_N < N_S$ and $t_N < t_S$). The noise-equivalent apertures are useful, e.g. when relating noise observed at a higher level to noise in underlying single photoreceptors. One consequence of the more restricted summation of noise is that SNRs of responses to full-field stimulation are higher than expected from signal-equivalent summation parameters, as if photons were summed over wider, "SNR-equivalent" areas and times ($N^* > N_S$ and $t^* > t_S$). This reflects the fact that (for the same potential responsivity to fine detail or fast changes) "smooth" weighting profiles collect less noise and thus reach higher SNRs than rectangular profiles when viewing images or time series with substantial autocorrelation (Tsukamoto et al., 1990; van Hateren, 1993).

Acknowledgments

This work was supported by the Academy of Finland (Grant 36154).

References

Adrian, E.D. & Matthews, R. (1927). The action of light on the eye. Part I. The discharge of impulses in the optic nerve and its relation to the electric changes in the retina. *Journal of Physiology* **63**, 378–414.

Aho, A.C., Donner, K., Hydén, C., Reuter, T. & Orlov, O.Yu. (1987). Retinal noise, the performance of retinal ganglion cells, and visual sensitivity in the dark-adapted frog. *Journal of the Optical Society of America A* **4**, 2321–2329.

Attwell, D. & Wilson, M. (1980). Behaviour of the rod network in the tiger salamander retina mediated by membrane properties of individual rods. *Journal of Physiology* **309**, 287–315.

Attwell, D., Borges, S., Wu, S.M., & Wilson, M. (1987). Signal clipping by the rod output synapse. *Nature* **328**, 522–524.

Barlow, H.B. (1956). Retinal noise and absolute threshold. *Journal of the Optical Society of America* **46**, 634–639.

Barlow, H.B. (1957). Increment thresholds at low intensities considered as signal/noise discriminations. *Journal of Physiology* **136**, 469–488.

Barlow, H.B. (1958). Temporal and spatial summation in human vision at different background intensities. *Journal of Physiology* **141**, 337–350.

Barlow, H.B. (1964). The physical limits of visual discrimination. In *Photophysiology, Vol. 2*, ed. Giese, A.C., pp. 193–203. London: Academic Press.

Barlow, H.B. (1977). Retinal and central factors in human vision limited by noise. In *Vertebrate Photoreception*, ed. Barlow, H.B. & Fatt, P., pp. 337–358. London: Academic Press.

Baumgardt, E. (1972). Threshold quantal problems. In *Handbook of Sensory Physiology, Vol. VII/4*, ed. Jameson, D. & Hurvich, L.M., pp. 29–55. Berlin: Springer.

Baylor, D.A. & Fettiplace, R. (1977). Kinetics of synaptic transfer from photoreceptors to ganglion cells in turtle retina. *Journal of Physiology* **271**, 425–448.

Baylor, D.A. & Hodgkin, A.L. (1973). Detection and resolution of visual stimuli by turtle photoreceptors. *Journal of Physiology* **234**, 163–198.

Baylor, D.A., Hodgkin, A.L. & Lamb, T.D. (1974). The electrical response of turtle cones to flashes and steps of light. *Journal of Physiology* **242**, 685–727.

Baylor, D.A., Matthews, G. & Yau, K.-W. (1980). Two components of electrical dark noise in toad retinal rod outer segments. *Journal of Physiology* **309**, 591–621.

BELGUM, J.H. & COPENHAGEN, D.R. (1988). Synaptic transfer of rod signals to horizontal and bipolar cells in the retina of the toad (Bufo marinus). *Journal of Physiology* **396**, 225–245.

BLOCH, A.M. (1885). Expériences sur la vision. *Compte Rendu de la Société de Biologie* **37**, 493–495.

CLELAND, B.G. & ENROTH-CUGELL, C. (1968). Quantitative aspects of sensitivity and summation in the cat retina. *Journal of Physiology* **198**, 17–38.

COPENHAGEN, D.R., DONNER, K. & REUTER, T. (1987). Ganglion cell performance at absolute threshold in toad retina: Effects of dark events in rods. *Journal of Physiology* **393**, 667–680.

COPENHAGEN, D.R., HEMILÄ, S. & REUTER, T. (1990). Signal transmission through the dark-adapted retina of the toad (*Bufo marinus*)—gain, convergence, and signal/noise. *Journal of General Physiology* **95**, 717–732.

DE VRIES, H. (1943). The quantum character of light and its bearing upon threshold of vision, the differential sensitivity and visual acuity of the eye. *Physica* **10**, 553–564.

DJUPSUND, K. (1995). *Measurement of the role of the photoreceptors in the retinal network*. Ph.D. Thesis, *Acta Universitatis Ouluensis D Medica 350*.

DJUPSUND, K. & HARIYAMA, T. (1995). The low-frequency voltage noise in the rod network of the dark-adapted frog. *Society for Neuroscience Abstracts* **21**, 1645.

DONNER, K. (1989). The absolute sensitivity of vision: Can a frog become a perfect detector of light-induced and dark rod events? *Physica Scripta* **39**, 133–140.

DONNER, K. & GRÖNHOLM, M.-L. (1984). Center and surround excitation in the receptive fields of frog retinal ganglion cells. *Vision Research* **24**, 1807–1819.

DONNER, K. & HEMILÄ, S. (1996). Modelling the spatio-temporal modulation response of ganglion cells with difference-of-Gaussians receptive fields: Relation to photoreceptor response kinetics. *Visual Neuroscience* **13**, 173–186.

DONNER, K., KOSKELAINEN, A., DJUPSUND, K. & HEMILÄ, S. (1995). Changes in retinal time scale under background light: Observations on rods and ganglion cells in the frog retina. *Vision Research* **35**, 2255–2266.

ENROTH-CUGELL, C. & LENNIE, P. (1975). The control of retinal ganglion cell discharge by receptive field surrounds. *Journal of Physiology* **247**, 551–578.

ENROTH-CUGELL, C., ROBSON, J.G., SCHWEITZER-TONG, D.E. & WATSON, A.B. (1983). Spatio-temporal interactions in cat retinal ganglion cells showing linear spatial summation. *Journal of Physiology* **341**, 279–307.

FAIN, G. (1975). Quantum sensitivity of rods in the toad retina. *Science* **187**, 838–841.

FAIN, G.L., GOLD, G.H. & DOWLING, J.E. (1976). Receptor coupling in the toad retina. *Cold Spring Harbor Symposia of Quantitative Biology* **40**, 547–561.

HARTLINE, H.K. (1940). The effects of spatial summation in the retina on the excitation of the fibers of the optic nerve. *American Journal of Physiology* **130**, 700–711.

LAMB, T.D. & SIMON, E.J. (1976). The relation between intercellular coupling and electrical noise in turtle photoreceptors. *Journal of Physiology* **263**, 257–286.

MINOR, A.V. & MAKSIMOV, V.V. (1969). Passive electrical properties of the model of a flat cell. *Biophysics* **14**, 349–357.

PUGH, E.N., JR. & LAMB, T.D. (1990). Cyclic GMP and calcium: The internal messengers of excitation and adaptation in vertebrate photoreceptors. *Vision Research* **30**, 1923–1948.

RICCÒ, A. (1877). Relazione fra il minimo angolo visuale e l'intensità luminosa. *Annali di Ottalmologia e Clinica Oculista* **6**, 373–479.

ROVAMO, J., RANINEN, A., LUKKARINEN, S. & DONNER, K. (1996). Flicker sensitivity as a function of spectral density of external white temporal noise. *Vision Research* **36**, 3767–3774.

ROVAMO, J., RANINEN, A. & DONNER, K. (1998). The effects of temporal noise and retinal illuminance on foveal flicker sensitivity. *Vision Research* (in press).

SCHWARTZ, E.A. (1975). Rod–rod interaction in the retina of the turtle. *Journal of Physiology* **246**, 617–638.

SCHWARTZ, E.A. (1976). Electrical properties of the rod syncytium in the retina of the turtle. *Journal of Physiology* **257**, 379–406.

SNEDECOR, G.W. & COCHRAN, W.G. (1967). *Statistical Methods*. Ames, Iowa: The Iowa State University Press.

SRINIVASAN, M.V., LAUGHLIN, S.B. & DUBS, A. (1982). Predictive coding: A fresh view of inhibition in the retina. *Proceedings of the Royal Society B* (London) **216**, 427–459.

TESSIER-LAVIGNE, M. & ATTWELL, D. (1988). The effect of photoreceptor coupling and synapse nonlinearity on signal: Noise ratio in early visual processing. *Proceedings of the Royal Society B* (London) **234**, 171–197.

TROY, J. (1993). Modelling the receptive fields of mammalian retinal ganglion cells. In *Contrast Sensitivity*, ed. SHAPLEY, R. & LAM, D.M., pp. 85–102. Cambridge, Massachusetts: The MIT Press.

TSUKAMOTO, Y., SMITH, R.G. & STERLING, P. (1990). "Collective coding" of correlated cone signals in the retinal ganglion cell. *Proceedings of the National Academy of Sciences of the U.S.A.* **87**, 1860–1864.

VAN DER ZIEL, A. (1970). *Noise Sources, Characterization, Measurement*. Englewood Cliffs, New Jersey: Prentice-Hall.

VAN HATEREN, J.H. (1993). Spatiotemporal contrast sensitivity of early vision. *Vision Research* **33**, 257–267.

Appendix

Simulation of signal and noise in the rod network of the toad retina

Signal simulations

A hexagonal rod lattice is shown in Fig. 3. The distance between nearest neighbors is a, each rod's interior is connected to the ground by a conductance G, and between each pair of nearest neighbors there is a resistance R. When the surface density of rods is ρ, the lattice constant is $a = \sqrt{(2/\sqrt{3})}/\sqrt{\rho} \approx 1.075/\sqrt{\rho}$. The leakage conductance is $G = G_s/\rho = (\sqrt{3}/2)G_s a^2$. The tangential resistance R can be easily calculated along the 12 symmetry axes. In both symmetry groups (six and six axes), $R = \sqrt{3}R_s$. Assuming that $a \ll \lambda$, the product RG is

$$RG \approx 1.5a^2 G_s R_s = 1.5(a/\lambda)^2 \tag{A1}$$

In *Bufo marinus*, $\rho \approx 15{,}000$ mm^{-2} and $\lambda \approx 20$ μm (Copenhagen et al., 1990). Thus, $a = 8.774$ μm, $a/\lambda = 0.439$, and $RG = 0.289$ with the asymptotic solution $U = U_B K_0(0.439\ r/a)$.

For calculating the voltages, we divide the lattice into 12 equal sectors (see Fig. 3A) and restrict the analysis to one sector. Due to the symmetry of the rod network, current never crosses sector borders. The lowermost resistors in Fig. 3B are on the border of two sectors, and this is taken into account by including two parallel resistors $2R$, one in each sector. Then the total resistance is R, but half of the current is flowing in each sector. Similarly, the leakage conductances of the rods along both sector borders are divided among two sectors and the conductance of the central cell is divided between 12 sectors. In each simulation, at least 50 rods were included in the sector network, corresponding to 481 rods in the whole RF. (Obviously, 50 rods × 12 sectors makes 600 rods, but it should be noted that the central rod is then included in each sector, i.e. counted 12 times instead of once, and, correspondingly, 18 "border" rods shared by neighboring sectors are counted 12 times instead of 6. This gives a corrected total of $[600 - 11 - (6 \times 18)]$ rods = 481 rods.) For normalized resistances, we used $R = 1\ \Omega$ and for corresponding conductances $G = 0.289$ S. A current I_0 (one twelfth of the total current) was injected into the midpoint. The sum of all currents at each junction is zero and the current in each resistor is voltage divided by resistance. The voltage of each rod (the voltage between a junction and the ground) was obtained by solving the resulting set of linear algebraic equations.

When calculating the currents in the peripheral resistances, the voltages of the rods in the periphery had to be known. Assuming that the modified Bessel function here describes the voltages well, eqn. (7) with $U_B = 1$ V was used to calculate these voltages. First, an arbitrary I_0 was used and the ratios U/K_0 at each rod were calculated. Then I_0 was iterated until U/K_0 was practically one in each rod except in the midpoint. After obtaining the

best fit with this current level, the voltages were normalized in order to obtain the relative responses $z(r)$:

$$z(r) = U(r)/U(0), \qquad 0 < z(r) < 1 \tag{A2}$$

Fig. 4 shows the normalized responses of the rods, i.e. the RF sensitivity profile $z(r)$. Except in the midpoint, the responses are well described by the function K_0. N_S is the sum of all normalized responses z. Taking into account the symmetry, the midpoint response is taken once, the responses on the sector borders six times, and all the other responses 12 times. The contribution of the small responses outside the calculated area is negligible. We obtain $N_S = 13.7$ rods and $A_S = N_S/\rho = 910\ \mu m^2$. Similarly, N_N is obtained by summing z_n^2, giving $N_N = 2.8$ rods, and finally $N^* = N_S^2/N_N = 67$ rods.

This simulation applies only to the values a and λ given above. Because K_0 is a function of the ratio r/λ, the N_S values of other rod mosaics should be proportional to $\rho\lambda^2$. However, this relation is not exact in the case of a discrete network. In fact, N_S is approximately proportional to $\lambda^{1.67}$ (Lamb & Simon 1976, Fig. 3).

Noise simulations

First, the variation of responses to weak full-field flashes was simulated, assuming that flashes produced 0.2 Rh^* on average. The normalized response contribution in the central rod caused by photoisomerizations in a rod at the distance r is $nz(r)$, where n is the number of photoisomerizations in each rod based on the Poisson distribution. The simulated total response is the sum of the contributions from all rods. In each simulation, the average response amplitude U and the mean square of the amplitudes, s^2 (estimator of the population variance σ^2), were determined based on 10,000 flashes. The SNR-equivalent number of rods was calculated by putting these estimates into eqn. (22). Two simulations gave the values $N^* = 67.8$ and 66.9 rods, in good agreement with the value $N^* = (\Sigma z_n)^2/\Sigma z_n^2 = 67$ rods. Note, however, that even when based on samples as large as 10,000, the N^* estimates varied by more than 1%. This variability is predominantly due to the relatively low precision in estimating population variance σ^2, which, moreover, improves but slowly with increasing sample size. Indeed, with samples typical in electrophysiological experimentation (<100), variability in s^2 will be on the order ±30% for statistical reasons alone (e.g. Snedecor & Cochran, 1967; cf. data in Table II of Copenhagen et al., 1990).

Second, the noise in the central rod due to quantal fluctuations of a full-field steady background light was simulated. "Independent activation" kinetics with $n = 4$ was assumed for the quantal response waveform. A background light intensity of $I_B = 0.2\ Rh^*s^{-1}$ was used, with photons distributed according to Poisson statistics on different rods and time intervals δt. Arbitrarily, we set $\delta t = 0.1$ s and $t_S = 1$ s for the simulation, the two are subject to the condition that $\delta t \ll t_S$. The voltage mean square s_B^2 obtained in the central rod was $0.371\ U_0^2$. (For the simulation, U_0 was arbitrarily set = 1 V, but the value is not important, since U_0 is eliminated in the calculation of N_N.) Setting $\sigma_B^2 = 0.371\ U_0^2$ in eqn. (12) gives the value $\Sigma z_n^2 = 2.73$ for N_N, in good agreement with the value $\Sigma z_n^2 = 2.8$ obtained above.